

Application research of contact network image detection based on support vector

Lihua Zhang

North China University of Water Resources and Electric Power, Henan Zhengzhou 45004, China
E-mail: lihuazhangqt@163.com

The complexity of the contact network parts and dramatic changes in the background environment make it difficult to detect the process. Based on this, this paper builds a corresponding support vector algorithm based on the kernel function to detect the image of the contact network. Meanwhile, this study establishes a support vector training model based on linear kernel, radial basis kernel and polynomial kernel. It is a single texture type training model based on linear kernel support vector method. In this study, the effectiveness of the kernel-based support vector method for insulator identification is verified by comparing the time and recognition performance of each model. At the same time, this study verifies the validity of the model by experimentally analyzing the spatial positioning accuracy of the mapping model. This provides a theoretical reference for subsequent related research.

1. INTRODUCTION

The most common and mature method for contact network detection applications today is contact detection. The method is mainly realized by a contact net detecting vehicle, and various parameters such as the height of the contact net, the offset of the contact line, the pressure between the bow nets, the hard point and the offline are detected by assembling various types of sensors on the detecting vehicle. After a long period of development, contact detection is constantly improving, but there are still some shortcomings: first of all, all kinds of detection will directly contact the wire, which will cause errors.

Secondly, contact inspection vehicles will occupy the road and affect the normal operation of high-speed trains. In par-

ticular, high-speed trains are now developing at a faster speed, with fewer trains, and generally operate during the day. Finally, there are some parameters that the test vehicle cannot measure, such as the angle of the positioner, the wear value of the contact line, the breakage of the insulator, and the foreign matter on the pillar.

In 1993, KIMURA et al. in Japan used ultrasonic ranging technology to achieve non-contact detection of bow network parameters (Wang, 2014). Zhang used laser-assisted image processing technology to design a vehicle monitoring system for wheel, brake pad and pantograph wear, which automates and increases labor productivity. Siemens in Germany developed an instrument that uses the principle of ultrasonic ranging to measure the height of the contact line and the position of the deviation (Zhang, 2015). In 2007, Japan used

image processing algorithms to develop a new system that extracts pantographs and trolley lines from images and calculates the three-dimensional position of contact points (Zhai, 2014). Yang et al. studied the pantograph contact line system with an infrared camera and implemented online monitoring of the bow network system using Hough line detection (Yang, 2015). She used three cameras to build an in-vehicle system that implements stereoscopic imaging technology, combined with infrared and ultraviolet light analysis, and finally it automatically detects foreign objects in the catenary suspension device (She, 2017). Pei first modeled the interaction between the pantograph and the contact net, and then divided the surface of the pantograph into three areas: safety, danger and fault.

Finally, the fault state of the system is analyzed by the number of contact points in each area, and the actual video image is used for real-time detection (Pei, 2017). Dong constructed a pantograph geometric model using images taken by the pantograph network and used the model to identify the type of pantograph (Dong, 2015). In order to measure the geometric parameters of the contact network in real time, Rajesh et al. developed a real-time measurement system based on the measurement principle of binocular vision, which has high measurement accuracy and high speed (Rajesh, 2015).

At present, the demand for contact network image detection is increasing. Although there are many researches and papers on actual contact network image detection, practical applications are rare. The main reason is the complexity of the contact network parts and the dramatic changes in the background environment (Hao, 2017), especially in high-speed conditions, making image processing and recognition very difficult. Therefore, this paper uses image detection based on support vector machine (support vector) as a tool to realize automatic detection of the contact network support device.

2. RESEARCH METHODS

Insulator detection technology based on computer vision image processing has been extensively studied as a non-contact detection method. Compared with the traditional manual method, the time consumption of the insulator cleaning work and the labor intensity of the inspection personnel are greatly reduced. Therefore, the identification of insulators through machine vision technology has become the research focus of high-voltage overhead transmission line maintenance and intelligent cleaning.

This article uses the most widely used Gaussian filtering. The Gaussian filter is often referred to as the most useful filter. It is a linear smoothing filter that selects weights based on the shape of a Gaussian function. The specific operation is to scan each pixel of the image with a template, and replace the value of the pixel just scanned with the weighted average of the pixels in the domain of the template. The two-dimensional discrete Gaussian functions commonly used in image processing are as follows:

$$G(x, y) = A \exp\left(\frac{-(x - u_x)^2}{2\sigma_x^2} - \frac{-(y - u_y)^2}{2\sigma_y^2}\right) \quad (1)$$

After the image is filtered, in order to accurately find the

position of the carbon slide, according to its contour feature, we need to perform edge detection on the image to extract the desired contour information. The Canny operator used to extract contours in this paper is a multi-level edge detection algorithm developed by John F. Canny in 1986 and is recognized as the best edge detection algorithm today. In order to meet the requirements of low error rate, high localization and minimum correspondence, the Canny algorithm uses a variational method. Similar to the sobel filter, the Canny algorithm obtains the possible edge points by calculating the magnitude and direction of the gradient (Shi, 2014). A pair of convolution arrays are applied to the x and y directions, respectively:

$$G(x) = \begin{bmatrix} -1 & 0 & 1 \\ -2 & 0 & 2 \\ -1 & 0 & 1 \end{bmatrix} \quad (2)$$

$$G(y) = \begin{bmatrix} -1 & -2 & -1 \\ 0 & 0 & 0 \\ 1 & 2 & 1 \end{bmatrix} \quad (3)$$

Then we use the following formula to calculate the gradient magnitude and direction separately:

$$G = \sqrt{G_x^2 + G_y^2} \quad (4)$$

$$\theta = \arctan\left(\frac{G_y}{G_x}\right) \quad (5)$$

The gradient direction generally takes four directions: 0 degrees, 45 degrees, 90 degrees, and 135 degrees. Some non-edge pixels are then excluded by maximal suppression, and only candidate edges are preserved. The hysteresis threshold is then utilized to determine the true boundary required. The study requires two thresholds: When the calculated pixel amplitude exceeds the high threshold, it remains as an edge; When the pixel value is lower than the low threshold, it is considered as a non-edge pixel, and is deleted; When the pixel amplitude is between the high threshold and the low threshold, it is retained as a boundary only when it is connected to a pixel above the high threshold.

By analyzing and training different kernel functions of support vector algorithm, a variety of visual recognition models are established, and the time-consuming and recognition accuracy of various kernel functions are compared. Considering that different model recognition speeds and recognition accuracy are not available, the research will select a recognition model with characteristics of speed and accuracy to establish a multi-core comprehensive recognition system.

Based on the multi-core support vector-based insulator visual recognition method and the recognition of the visual characteristics of the insulator, the multi-core support vector algorithm is used to perform multi-identification and comprehensive evaluation of the sample. The main research contents are: 1) Visual feature recognition of insulators. Experiments were carried out on the spatial structure, texture, color and gradient distribution of the insulator to evaluate the effective degree of each characteristic parameter. The available feature parameters were processed by principal component analysis to establish a feature sample suitable for post processing. 2) Research also focused on multi-core support vector learning

methods. Insulator feature samples are learned by kernel functions such as linear kernel, RBF kernel, polynomial kernel, etc. The training time and accuracy under different kernel function support vector algorithms are statistically calculated. 3) Parameter optimization based on group intelligent optimization algorithms. By summarizing the parameter distribution law of support vector algorithm, a suitable heuristic group intelligent search algorithm is selected. This permits us to optimize the multi-parameters of the penalty factors and kernel coefficients of the support vector to improve the training model.

The training sample is assumed to be a set of samples to be classified containing insulator targets and non-insulator interference targets. x represents a visual feature sample whose target is an insulator, and o represents a corresponding visual feature sample whose target is a non-insulator interference object. Moreover, to establish the insulator visual recognition mode, it is necessary to find a classification line H to completely separate the visual characteristic values of the insulator and the non-insulator interference object. For the entire feature sample input space applied to the insulator visual feature recognition, H can be used as the optimal classification surface for this high-dimensional space. A set of feature data is set to $\{(x_i, y_i), i = 1, 2, \dots, n\}$, and the optimal classification line available in the two-dimensional space is equation (6). Similarly, for the high-dimensional space of the insulator visual feature sample, the straight line H_1 and H_2 passing through the visual feature sample closest to the classification surface are expressed as equation (7). The constant term parameter b is adjusted to obtain equation (8). The optimal classification surface of the insulator visual feature in high dimensional space is

$$f(x, b) = \langle w \cdot b \rangle + b \quad (6)$$

$$H_1 \langle w \cdot x \rangle + b = k_1 \quad H_2 \langle w \cdot x \rangle + b = k_2 \quad (7)$$

$$H_1 \langle \cdot x \rangle + b = -k \quad H_2 \langle w \cdot x \rangle + b = k \quad (8)$$

The optimal classification surface of the insulator visual feature in high dimensional space is $H \langle w \cdot x \rangle + b = k_1$. Letting $\tau = \frac{w}{k}$, $\rho = b/k$, then H_1 and H_2 can be expressed as equation (9).

$$H_1 \tau \cdot x + \rho = -1 \quad H_2 \tau \cdot x + \rho = 1 \quad (9)$$

Therefore, the ‘‘interval’’ of the insulator visual feature sample boundaries H_1 and H_2 is $\max\{|(2)|\}$. The constraint condition for visually identifying the optimal solution for this insulator is: 1) When the target is an insulator, ie, $y_i = 1$, $w \cdot x_i + b \geq 1$. 2) When the target is a non-insulator interference term, ie, $y_i = -1$, $w \cdot x_i + b \leq -1$. The objective function can be defined as equation (10), and the penalty factor C and the relaxation variable ξ_i can be introduced to represent the objective function as equation (11). The Lagrange equation is constructed and transformed into a quadratic pro-

gramming problem. This can be seen in equation (12).

$$\begin{cases} \min \frac{1}{2} \|w\|^2 \\ s.t. y_i(w \cdot x_i + b) \geq 1, \quad i = 1, 2, \dots, l \end{cases} \quad (10)$$

$$\begin{cases} \max_{w,b,\xi} \frac{1}{2} \|w\|^2 + C \sum_{i=1}^n \xi_i \\ s.t. y_i w \cdot x_i + b \geq 1 - \xi_i, \quad \xi_i \geq 0, \quad i = 1, 2, \dots, n \end{cases} \quad (11)$$

$$L(w, b, \xi_i, \alpha, \beta) = \frac{1}{2} \|w\|^2 + C \sum_{i=1}^n \xi_i - C \sum_{i=1}^n \alpha_i (y_i (w^T x_i + b) - 1 + \xi_i) - \sum_{i=1}^n \beta_i \xi_i \quad (12)$$

Among them, $\alpha_i, \beta_i, i = 1, 2, \dots, n$ is Lagrangian multipliers. According to the saddle point theorem, the Lagrangian equation is solved by using L , partial derivative of w, b , and ξ_i respectively to obtain the equation (13). Equation (13) is substituted into equation (12) to get the dual problem. The result can be seen in equation (14). The dual equation (14) is solved to obtain the final decision function, that is, the insulator visual recognition model, as shown in equation (15). In the formula, $K(x_i, x_j)$ is a kernel function that satisfies the Hilbert-Schmidt theorem and the Mercer condition.

$$\begin{cases} W = \sum_{i=1}^n \alpha_i y_i x_i \\ C - \alpha_i - \beta_i = 0 \\ \sum_{i=1}^n \alpha_i y_i = 0 \end{cases} \quad (13)$$

$$\begin{cases} \max_{\alpha, \beta} \sum_{i=1}^n \alpha_i - \frac{1}{2} \sum_{i=1}^n \sum_{j=1}^n \alpha_i \alpha_j y_i y_j \langle x_i \cdot x_j \rangle \\ s.t. \sum_{i=1}^n \alpha_i y_i = 0, \quad 0 \leq \alpha_j \leq C \\ f(x) = \text{sgn}(\sum_{x=sv} \alpha_i K(x_i, x_j) + b) \end{cases} \quad (14)$$

The Lagrangian multiplier solved in equation (14) corresponds to the insulator characteristic $\langle x_i \cdot x_j \rangle$. It is known from the inequality relation of the formula (10) that it needs to satisfy the KKT (Karush-Kuhn-Tucker) condition, that is,

$$\begin{cases} a_i \geq 0 \\ y_i f(x_i) - 1 \geq 0 \\ a_i (y_i f(x_i) - 1) = 0 \end{cases} \quad (15)$$

According to the KKT condition, there is always $a_i = 0$ or $y_i f(x_i) = 1$ for training arbitrary samples. Therefore: 1) When $a_i = 0$, the sample has a value of 0 in the sum of equations (15) and does not affect $f(x_i)$. When $a_i \geq 0$, then $y_i f(x_i)$, indicating that the sample is at the maximum interval boundary and is a support vector. It can be seen from the above conditions that the support vector machine algorithm does not need to save all sample values after training the sample. The final model (15) is only related to the support vector.

3. RESULTS

Aiming at the problem that the calibration samples in the current camera indirect calibration method are incomplete and the model expression is fuzzy. In this study, a hexagonal lattice calibration plate readable by the target number and a support vector algorithm based on structural risk minimization are used. A support vector calibration method based on full-view sampling of the binocular system is proposed.

At the same time, this study analyzes the calibration model and verifies the feasibility of the method. The schematic diagram of the experimental equipment constructed in this study is shown in Figure 1.

The full-view sampling calibration experiment uses a 640×480 USB-driven camera, and the world coordinate system is set by default to the center of the calibration plate. The specific process is: 1) Installation of binocular vision system and calibration plate lifting equipment. 2) The calibration plate and the binocular vision system are adjusted so that the center of the calibration plate is in the image acquired by the two cameras and has a large image intersection. 3) The lifting table is adjusted and the calibration sample is collected at the current position. 4) The lifting platform is gradually raised by 5 mm up to a height of 50 mm, and step 3 is repeated. After that, the lifting platform is gradually lowered by 5 mm, and step 3) is repeated, thereby reducing the error. A sample of the calibration plate collected by the binocular vision system is shown in Figure 2.

In order to compare this with the traditional sampling method, taking the calibration plate sample points collected at 50mm as the standard, we select 252 detection points from all the samples to establish the sample 1 (This is shown in Figure 2(a)). The full-view sampling sample considers the sample size and the sampling detection principle to select 568 detection points to establish the sample 2, as shown in Figure 2(b). At the same time, 568 test points in the total sample were taken as test samples of the two methods for the later precision test.

The acquired detection points are taken as input on the virtual plane coordinates (U_1, V_1, U_2, V_2) of the left and right cameras. Their world coordinates (X^1, Y^1, Z^1) are taken as outputs. The sample is trained by the support vector to construct three axial output models, so that the final calibration model can achieve a given input-output mapping relationship. In the MATLAB environment, the linear kernel function support vector algorithm training samples are used to obtain the calibration model. model.rho represents the constant term in the model, and model.sv_coef represents the support vector coefficient in the model. The constant mathematical term, the support vector coefficient, and the support vector are substituted into the objective function to obtain the specific mathematical models of X^1 , Y^1 , and Z^1 , respectively.

In the support vector algorithm, the prediction accuracy of the model established by different penalty factors is different, so choosing the appropriate penalty factor is the key to establish a good calibration model. In the experiment, the calibration model of the X, Y and Z axes was established by the optimization algorithm [58] with the penalty factors of 0.65, 0.45 and 0.95. In order to verify the effectiveness of the penalty factor, the comparison model is established by using: different penalty factors, coefficient of determination, mean square error and mutual correlation. These are used as evaluation indicators for comparative analysis. In order to verify the effectiveness of the penalty factor, the comparison model is established by using different penalty factors, and the comparison coefficient is determined by determining the coefficient, the mean square error and the cross-correlation coefficient. The results are shown in Table 2, Table 3, Table 4, and Figure

4.

In Fig. 3, the abscissa is the position of the detection point on the coordinate axis, and the ordinate is the average error between the world coordinates mapped by the calibration model on the scales of the coordinate axes and the actual world coordinates. From Fig. 3, the calibration model can be obtained when the penalty factor has the values 0.65, 0.45, and 0.95. The reconstruction position and the actual coordinate position of the detection point are smaller than the average error of the calibration model constructed by other values. From Table 2 to Table 4, it can be concluded that in the establishment of three axial output models, when the penalty factor is 0.65, 0.45, 0.95, and the established calibration model is compared with other calibration models, the mean square error of the reconstructed coordinate position and the actual coordinate position is smaller and the cross-correlation is stronger. The results show that the penalty factor obtained by the optimization algorithm has higher calibration accuracy than the calibration model established by other penalty factors.

In this case the validity of the selected parameters is verified.

The sample 1 acquired by the traditional sampling method is built with the same optimization algorithm to establish a calibration model based on the support vector and compared with the calibration model established by the method. Meanwhile, the plane coordinate 4 coordinate values (U_1, V_1, U_2, V_2) are respectively converted into world coordinate three-coordinate values (X^1, Y^1, Z^1) and the results are shown in Fig. 4 and Table 5. In Fig. 5, the abscissa is the position of the detection point on the coordinate axis, and the ordinate is the error rate distribution of the reconstructed coordinate value. In addition to this the actual coordinate value of the detection point is at each position. In Table 5, the two models are quantified by determining the coefficient, mean square error, and cross-correlation coefficient.

4. DISCUSSION AND ANALYSIS

In Figure 2, the first frame is the sample collected by the camera when the calibration plate is at 0 mm, and the 11th frame is the sample collected by the camera when the calibration plate is at 50 mm. In the process of obtaining the sample point number and coordinate value collected in the calibration plate, DataID , CameraIdx , ObjIdx , and ObjPoseIdx are input parameters as indexing numbers of the calibration model, the observation camera group, the calibration target, and the calibration target position. In the output parameters, Index is the number of the detection point on the calibration board, Row is the row coordinate of the detection point in the image, Column is the column coordinate of the detection point in the image, and Pose is the relative position of the calibration object and the camera. Based on the binocular system, the detection point number is acquired, and the target plane 4 coordinates (U_1, V_1, U_2, V_2) and the world coordinate values (X^1, Y^1, Z^1) on the calibration plate are acquired. A total of 2839 detection points are effectively collected, as shown in Table 1. Each detection point contains information such as left and right image horizontal and vertical coordinates and world coordinates. Among them, the plane 4 coordinate value unit is a pixel, that is, the pixel coordinates of the image taken

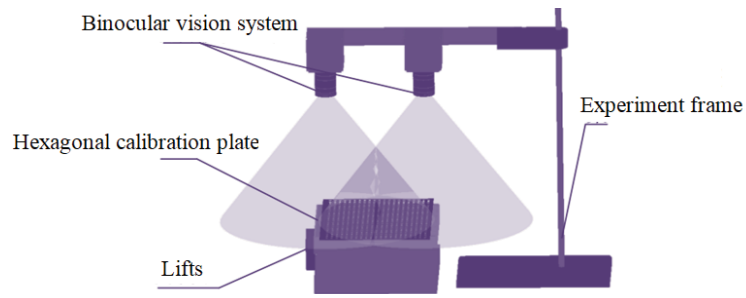


Figure 1 Schematic diagram of the experimental equipment.

Table 1 Partial samples collected by the binocular vision system.

Serial number	Actual coordinates /mm			Left camera		Right camera	
	X	Y	Z	U1	V1	U2	V2
a	-38.707	67.049	5.00	36.335	21.968	429.379	45.162
b	-34.836	60.344	10.00	40.774	34.83	443.762	58.216
c	-38.707	53.639	15.00	19.34	47.334	436.09	71.091
d	-27.094	46.935	20.00	41.623	60.256	476.775	83.872
e	-23.223	40.23	25.00	38.733	73.05	496.934	96.712
f	-19.352	33.525	35.00	32.71	84.073	522.248	107.795
g	-15.481	26.82	40.00	61.94	102.694	571.255	126.306
h	-19.352	20.116	45.00	9.796	121.318	536.623	145.509

Table 2 Error Analysis (X-Axis).

Serial number	Penalty factor	Decisive factor	Mean square error	Cross correlation coefficient
1	0.552	0.997	1.495	0.999
2	0.652	0.997	1.452	0.999
3	0.752	0.997	1.483	0.999
4	2.602	0.997	1.64	0.999

Table 3 Error Analysis (Y-axis).

Serial number	Penalty factor	Decisive factor	Mean square error	Cross correlation coefficient
1	0.352	0.994	13.018	0.998
2	0.452	0.994	12.768	0.998
3	0.552	0.994	12.997	0.998
4	1.802	0.994	13.037	0.998

Table 4 Error Analysis (Z-Axis).

Serial number	Penalty factor	Decisive factor	Mean square error	Cross correlation coefficient
1	0.852	0.993	1.635	0.997
2	0.952	0.993	1.618	0.997
3	1.052	0.993	1.636	0.997
4	3.802	0.992	1.825	0.997

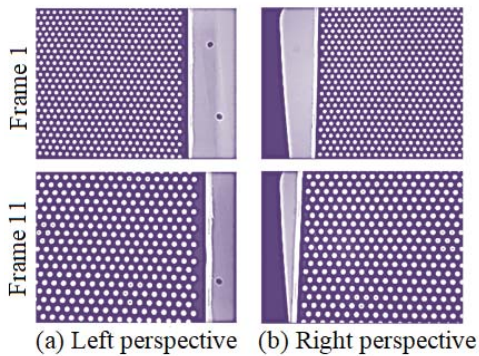
by the target point in the left and right view.

The support vector machine algorithm based on kernel function is applied to the visual recognition task of insulators, and the insulator visual recognition model is established based

on linear kernel, radial basis kernel, polynomial kernel and different single characteristic linear kernels.. By comparing and analyzing the time and recognition performance of each model, this study verifies the validity of the kernel-based sup-

Table 5 Comparison and analysis of calibration results of two sampling methods.

Sampling method		Decisive factor	Mean square error	Cross correlation coefficient
Traditional sampling	X	0.995	2.043	0.997
	Y	0.992	16.948	0.996
	Z	0.991	1.694	0.995
Full view sampling	X	0.995	1.450	0.997
	Y	0.992	12.766	0.996
	Z	0.991	1.616	0.995

**Figure 2** Samples collected by the binocular vision system.

port vector method for insulator identification and determines the multi-core insulator visual recognition model based on LBP, HOG linear kernel, and support vector model based on full sample linear kernel, radial basis kernel and polynomial kernel.

The performance impact of parameters on the final recognition model in the support vector method based on kernel function is analyzed. By comparing the Gaussian normal distribution function, this study explains the role of the support vector number in the model prediction, and determines the performance of the model by the model identification accuracy and the number of support vectors. Meanwhile, through the classification algorithm to reconcile the averaging function, this study proposes a support vector model performance evaluation function. In addition, this study conducts an experimental analysis of a variety of swarm intelligence optimization algorithms to determine the parameters of the support vector kernel function method by differential evolution algorithm. On the basis of ensuring the recognition accuracy of the final insulator visual recognition model, this study reduces the number of radial basis kernel support vectors to 62, and the number of polynomial kernel support vectors to 239.

An insulator binocular vision spatial positioning system is established. Meanwhile, the hexagonal lattice calibration plate and HALCON operator are used to realize the full-view sampling of the binocular vision system, and the mapping model of the two-dimensional target to the three-dimensional spatial position is established by the support vector algorithm. Through the experimental analysis, the calibration error of the model established by the traditional sampling method is reduced by 24.51%, which verifies the validity of the model and combines with the insulator visual recognition model to realize the spatial positioning of the insulator.

In this project, a visual recognition model based on kernel function support vector algorithm is established in the research of insulator visual recognition, but it also has the following shortcomings: (1) Target extraction with interference insulators achieves accurate target segmentation extraction in the laboratory environment, but in the actual environment due to changes in sunlight, shooting angles and other environmental factors, the insulator target is incompletely extracted or carries background interference. By improving the performance of the insulator extraction algorithm and training with the insulator image samples with interference, the anti-interference of the final recognition model can be further improved. (2) When the differential evolution algorithm is iterative, the long-term insulator visual recognition model uses the differential evolution algorithm to optimize the support vector kernel function parameters. However, when the optimization iteration is too long, the performance is not completely leading in the test function comparison. Improving the computational speed of the differential evolution algorithm can further improve the construction efficiency of the insulator visual model. (3) The visual model of the insulator to be further enriched is composed of Hu invariant moment, LBP descriptor, HOG descriptor, Haar descriptor, but the target texture description operator with better performance will be proposed with the development of target recognition technology. The timely adoption of new research theories can further improve the visual recognition performance of insulators.

5. CONCLUSION

In this paper, the visual recognition system of the contact net insulator is studied, and the Canny operator used for the contour is extracted. By analyzing and training different kernel functions of support vector algorithm, a variety of visual recognition models are established, and the time-consuming and recognition accuracy of various kernel functions are compared. Considering that the recognition speed and recognition accuracy of different models are not available, the identification model with characteristics of speed and accuracy is selected to establish a multi-core comprehensive recognition system. In this paper we aim to resolve the problem that the calibration samples in the current camera indirect calibration method are incomplete and the model expression is fuzzy. For this purpose this study utilizes a hexagonal lattice calibration plate readable by the target number and a support vector algorithm based on structural risk minimization. Meanwhile, this study proposes a support vector calibration method based on

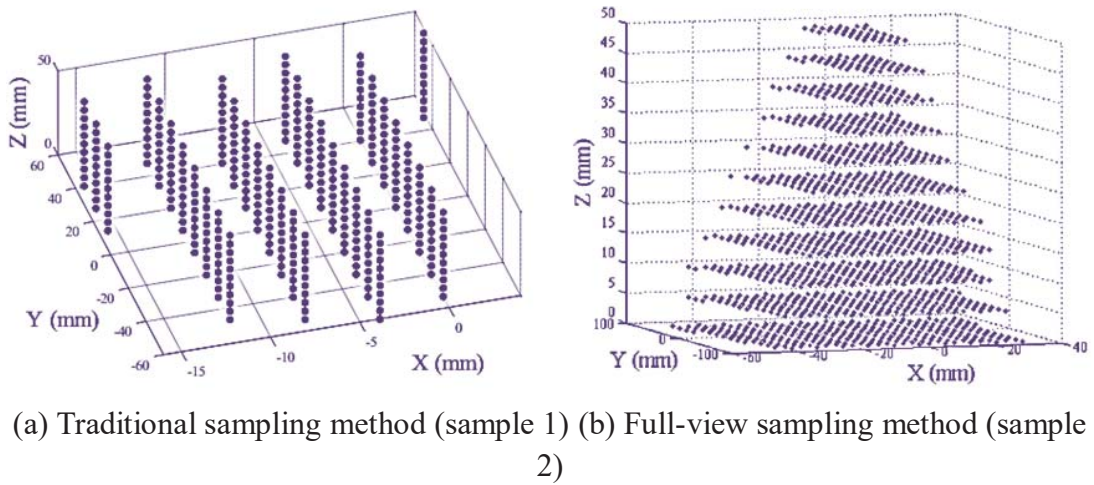


Figure 3 Sample distribution under different methods.

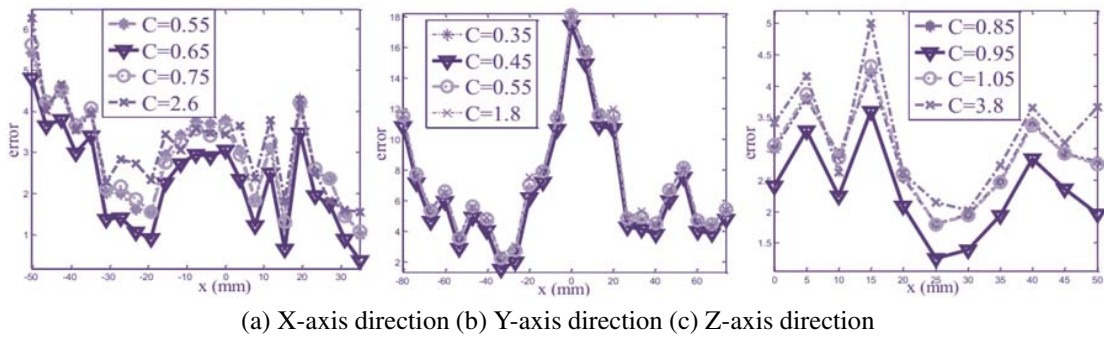


Figure 4 Model analysis of different support vector parameters.

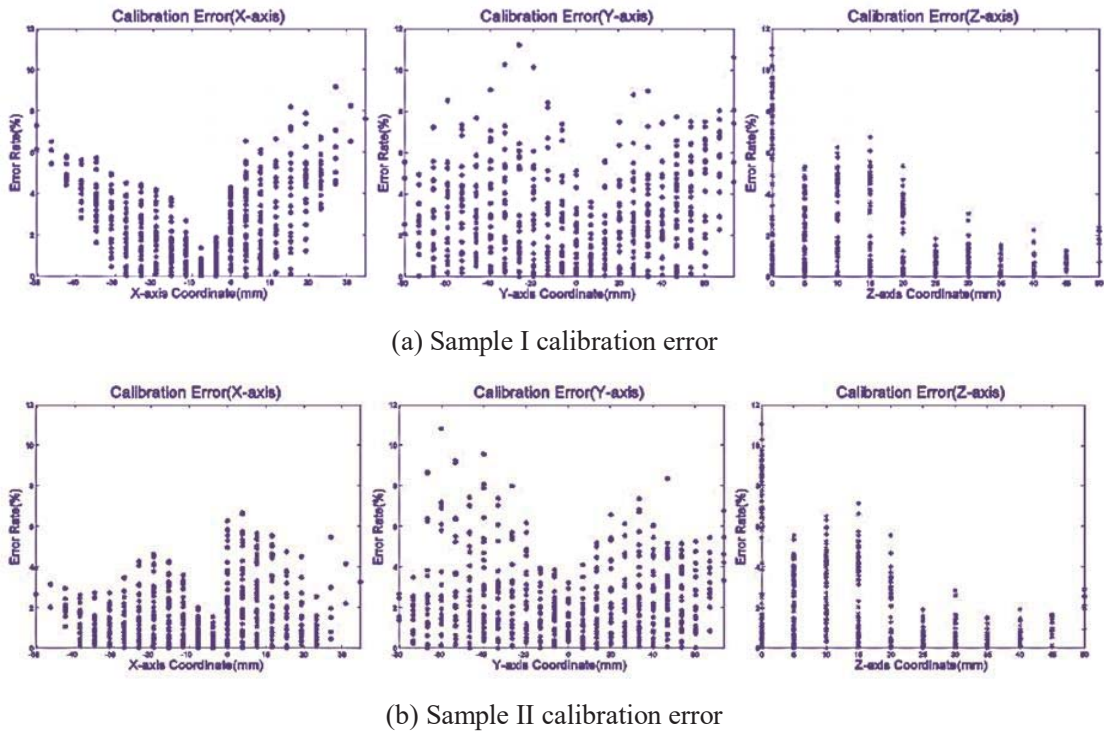


Figure 5 Comparison analysis of error distribution between two sampling methods.

full-view sampling of binocular system and analyzes the calibration model to verify the feasibility of the method. In this study, the support vector machine algorithm based on kernel function is applied to the visual recognition task of insulators, and the insulator visual recognition model based on linear kernel, radial basis kernel, polynomial kernel and different single characteristic linear kernels is established. By comparing and analyzing the time and recognition performance of each model, the validity of the kernel-based support vector method for insulator identification is verified. At the same time, the penalty factor obtained by the optimization algorithm in this paper has higher calibration accuracy than the calibration model established by other penalty factors, and the validity of the selected parameters is verified.

REFERENCES

1. Wang Y, Guo H. Weld Defect Detection of X-ray Images Based on Support Vector Machine[J]. Iete Technical Review, 2014, 31(2):137-142.
2. Zhang T, Wang J. Network intrusion detection based on cooperative quantum-behaved particle swarm algorithm and least square support vector machine[J]. Computer Engineering & Applications, 2015, 13(4):350-360.
3. Zhai J. Research on Intrusion Detection System Based on Clustering Fuzzy Support Vector Machine[J]. International Journal of Security & Its Applications, 2014, 8(3):249-260.
4. Yang K, Zhang R, Yang J, et al. Research on Low-voltage Series Arc Fault Detection Method Based on Least Squares Support Vector Machine[J]. Open Electrical & Electronic Engineering Journal, 2015, 9(1):408-421.
5. She C, Wen W, Lin Z, et al. Application-Layer DDOS Detection Based on a One-Class Support Vector Machine[J]. International Journal of Network Security & Its Applications, 2017, 9(1):13-24.
6. Pei L R, Jiang P P, Yan G Z. Research on fall detection system based on support vector machine[J]. Optics & Precision Engineering, 2017, 25(1):182-187.
7. Wang L, Dong C, Hu J, et al. Network Intrusion Detection Using Support Vector Machine Based on Particle Swarm Optimization[J]. Plant Biotechnology Reports, 2015, 4(3):237-242.
8. Rajesh T, Malar R S M. Rough set theory and support vector machine classifier based brain tumor detection of MR images[J]. International Journal of Applied Engineering Research, 2015, 10(8):19331-19344.
9. Dong L, Chen L, Hao J. Soft multimedia anomaly detection based on neural network and optimization driven support vector machine[J]. Multimedia Tools & Applications, 2017(10):1-24.
10. Yang J, Shi Y, Zhou W, et al. Study on Detection Method for Crack in Eggs Based on Computer Vision and Support Vector Machine Neural Network[J]. Applied Mechanics & Materials, 2014, 472:176-179.

Lihua ZHANG, coming from Shenyang City, Liaoning Province, was born in 1971. She has a Master's degree and senior position. Her main research interests is in Computer Science and Technology, and Information Security.